materials

MDPI

Article

Enhanced Charge Extraction of Li-Doped TiO_2 for Efficient Thermal-Evaporated Sb_2S_3 Thin Film Solar Cells

Chunfeng Lan [1,2,3,†], Jingting Luo [1,3,†], Huabin Lan [1,3], Bo Fan [1,3], Huanxin Peng [1,3], Jun Zhao [1,3], Huibin Sun [1,2], Zhuanghao Zheng [1,3], Guangxing Liang [1,3,*] and Ping Fan [1,3,*]

1 Shenzhen Key Laboratory of Advanced Thin Films and Applications, College of Physics and Energy, Shenzhen University, Shenzhen 518060, China; lanchunfeng@gmail.com (C.L.); luojt@szu.edu.cn (J.L.); lanhb420@163.com (H.L.); fanb07@hotmail.com (B.F.); P2385284535@163.com (H.P.); zhaojun@szu.edu.cn (J.Z.); hbsun@szu.edu.cn (H.S.); zhengzh@szu.edu.cn (Z.Z.)

2 Key Laboratory of Optoelectronic Devices and Systems of Ministry of Education and Guangdong Province, College of Optoelectronic Engineering, Shenzhen University, Shenzhen 518060, China

3 Institute of Thin Film Physics and Applications, College of Physics and Energy, Shenzhen University, Shenzhen 518060, China

* Correspondence: lgx@szu.edu.cn (G.L.); fanping@szu.edu.cn (P.F.)

† These authors contributed equally to this work.

Received: 16 January 2018; Accepted: 26 February 2018; Published: 28 February 2018

Abstract: We provided a new method to improve the efficiency of Sb_2S_3 thin film solar cells. The TiO_2 electron transport layers were doped by lithium to improve their charge extraction properties for the thermal-evaporated Sb_2S_3 solar cells. The Mott-Schottky curves suggested a change of energy band and faster charge transport in the Li-doped TiO_2 films. Compared with the undoped TiO_2, Li-doped mesoporous TiO_2 dramatically improved the photo-voltaic performance of the thermal-evaporated Sb_2S_3 thin film solar cells, with the average power conversion efficiency (*PCE*) increasing from 1.79% to 4.03%, as well as the improved open-voltage (V_{oc}), short-circuit current (J_{sc}) and fill factors. The best device based on Li-doped TiO_2 achieved a power conversion efficiency up to 4.42% as well as a V_{oc} of 0.645 V, which are the highest values among the reported thermal-evaporated Sb_2S_3 solar cells. This study showed that Li-doping on TiO_2 can effectively enhance the charge extraction properties of electron transport layers, offering a new strategy to improve the efficiency of Sb_2S_3-based solar cells.

Keywords: Li-doping; charge extraction; thermal evaporation; Sb_2S_3 solar cells; photovoltaic performance

1. Introduction

Investigation of low-cost, abundant, and efficient absorbing materials is one of the most important issues for solar cell applications. From this aspect, chalcogenide compounds, such as Sb_2S_3, Sb_2Se_3, have attracted considerable attention in recent years [1–6]. Compared to Sb_2Se_3, Sb_2S_3 exhibits some unique merits, such as the tunable band-gap with high absorption coefficient, easy processing, stability and with abundant raw materials [2–5]. More importantly, the Sb_2S_3-based solar cells show excellent photovoltaic performance in weak light illumination conditions, which makes it feasible to achieve efficient power conversion in cloudy days or indoor conditions [7]. Therefore, the research on high-performance Sb_2S_3 solar cells is still of high value.

The Sb_2S_3 films for solar cells application have been prepared by thermal evaporation and chemical deposition method [3,8–12]. Compared to the chemical deposition, thermal evaporation shows some unique advantages, e.g., compatibility with future fabrication of large-area solar cells [8,12]. However, so far, the thermal-evaporated Sb_2S_3 thin film solar cells only showed a highest *PCE* of 3.01%, which is lower than that of chemical deposition method [10,12]. The thermal-evaporated Sb_2S_3

solar cells are still encountering the problem of low *PCE*, as well as the low short-circuit current and open-circuit voltage [10,11]. How to improve their photovoltaic performance remains a priority for Sb_2S_3 solar cells [7,13–15]. It is reported that besides the film quality of absorbing layers, low charge extraction was another important factor affecting the power conversion of devices. In particular, the transport efficiency of photo-excited electrons from the absorbing layer to the electron transport layer was very low on the Sb_2S_3/TiO_2 interface, which impeded the improvement of the power conversion efficiency [16]. To overcome this limitation, some new materials and structures have been introduced into the Sb_2S_3 solar cells, such as ZnO and ZnO cored TiO_2 rods as electron transport layers to enhance the charge extraction process [17–20]. Unfortunately, so far few of the Sb_2S_3 solar cells based on these materials or structures reached a satisfying *PCE*, leaving many challenges for future development [17–20]. Thus, new strategies are required to raise the photovoltaic performance of Sb_2S_3 solar cells. Recently, doping of TiO_2 layer has been reported as an effective method to improve the charge extraction in perovskite solar cells [21–23]. This gives us an inspiration for the improvement of Sb_2S_3/TiO_2-based solar cells.

In this work, we use the thermal-evaporated Sb_2S_3 thin films as absorbing layers and Li-doped TiO_2 as charge transport layers to fabricate the solar cells, and we find that Li-doping dramatically improves the photovoltaic performance of Sb_2S_3 solar cells, with an average *PCE* of 4.03%, as well as a champion *PCE* up to 4.42% and V_{oc} of 0.645 V, offering an efficient method to raise the photovoltaic performance of thermal-evaporated Sb_2S_3 solar cells.

2. Experimental

2.1. Preparation of Sb_2S_3 Thin Film and Li-Doped TiO_2

Sb_2S_3 thin films were thermally evaporated on corning glass substrates or TiO_2-coated fluorine-doped SnO_2 glass (2.0 × 2.0 cm^2, fluorine-doped tin oxide (FTO) glass, Sigma-Aldrich, Saint Louis, MO, USA) under a high vacuum (1.5 × 10^{-3} Pa) using 0.5 g of commercial Sb_2S_3 powder (99.999%, Sigma Aldrich). The evaporation was carried out at room temperature. After the evaporation, the as-deposited films were immediately transferred into N_2 glove box and annealed on hot plate at 275 °C for 10 min. As mentioned in reference [24], the TiO_2 precursor was spin-coated on the corning glass and FTO glass respectively, and then sintered at 450 °C for 30 min to form a compact layer. TiO_2 paste (30NR-D, Dyesol, Queanbeyan, Australia) diluted by alcohol (weight ratio of 1:6) was spin-coated on a dense TiO_2 compact layer, and then sintered at 450 °C for 30 min to form a mesoporous structure. For the Li-doped mesoporous TiO_2, 0.05, 0.1, 0.2 M bis (trifluoromethane) sulfonimide lithium salt (Li-TFSI) (99.9%, Macklin, Shanghai, China) in acetonitrile solutions were spin coated on the meosporous TiO_2 layers respectively (with the Li-TFSI salt concentration higher than 0.2 M, the homogeneity of the TiO_2 film was sharply reduced, thereby the concentration of Li-TFSI salt used was not higher than 0.2 M), and again sintered at 450 °C for 30 min to form Li-doped TiO_2. After cooling to 150 °C, the substrates were immediately transferred into the thermal evaporator for the deposition of Sb_2S_3 thin films.

2.2. Device Fabrication

FTO glass was cleaned by isopropanol, acetone, de-ionized water, and alcohol in ultrasonic cleaner, dried and then treated by ultraviolet ozone treatment before use. Li-doped TiO_2 films were prepared on cleaned FTO glass as described above. In addition, then the Sb_2S_3 films were thermally evaporated on them and annealed in an N_2 atmosphere glove box. 72.3 mg of Spiro-OMeTAD in 1 mL of chloridebenze solution was used as hole transport materials with the addition of 28 μL of 4-tert-butylpyridine and 19 μL of TSFI-Li acetonitrile (520 mg/mL). It was spin coated on the Sb_2S_3 films at a speed of 3000 rpm for 30 s. Finally, 50 nm of Au film was deposited as top electrode by thermal evaporation. The devices fabricated on the different Li-doped TiO_2 were labeled as undoped TiO_2, 0.05Li + TiO_2, 0.1Li + TiO_2 and 0.2Li + TiO_2.

2.3. Characterization

The phase structure of the films was analyzed using powder X-ray diffraction (XRD) (Ultima IV, Rigaku, Tokyo, Japan) with Cu*Kα* radiation (λ = 0.15406 nm) operated at 40 kV and 40 mA. The surface morphology and cross-section of prepared films and devices was analyzed by field-emitted scanning electron microscopy (FE-SEM) (SUPRA 55, Zeiss, Oberkochen, Germany). The composition of the film was mapped by the energy dispersive x-ray microanalysis system (EDX) (Bruker QUANTAX 200, Bruker, Billerica, MA, USA). X-ray photoelectron spectroscopy was measured by using a system (PHI 5000 Versa Probe II, Ulvac-Phi, Chigasaki, Japan) with a monochromatic Al *Kα* X-ray source (1486.7 eV) at 50 W and 16 kV with a beam spot size of 200 μm. UV-visible spectra measurement was performed by a spectrophotometer (UV-3600Plus, Shimadzu, Japan). Mott-Schottky measurement was carried out using an electrochemical workstation (CHI660E, CH Instruments, Shanghai, China) with the structure of FTO/TiO_2, at a scan rate of 10 mV·s^{-1}. Current density-voltage (*J-V*) characteristics of the Sb_2S_3 solar cells were tested under simulated AM 1.5G conditions (100 mW/cm^2) with a Keithley 2400 sourcemeter in ambient condition in-house. The voltage was scanned from 0 to 1 V with a scan rate of approximately 0.1 V/s. Devices area illuminated were precisely set by a mask with an area of 0.08 cm^2. External quantum efficiency (EQE) was measured with the photoelectric conversion test system (SCS100-X150-DSSC, Zolix Instruments, Beijing, China) with a standard silicon solar cell as reference.

3. Results and Discussion

With the Li-TFSI deposition and sintering processes, the introduction of lithium lead to the different surface states of mesoporous TiO_2 layers, such as the formation of LiO_2, LiOH or $Li_4Ti_5O_{12}$ [25,26], which sharply affects the electron extraction properties of the TiO_2 layer in the perovskite solar cells. To study the elemental states in the undoped and Li-doped mesoporous TiO_2 layers, X-ray photoelectron spectroscopy (XPS) was applied to characterize the elemental compositions. Figure 1 shows the fitted XPS patterns of the TiO_2 and the 0.2 M Li-doped TiO_2 films. Generally speaking, the XPS intensity of the Li-doped TiO_2 is apparently weaker than that of the undoped samples, inferring that the surface state of TiO_2 layers has been changed by the lithium-treatment. In detail, in Figure 1a there is a slight shoulder at the peak near 530 eV in the XPS patterns of the Li-doped TiO_2 film, where the peak is related to the O1s spectra [22]. The peak deconvolution suggests that this shoulder originated from the interaction of the oxygen and the lithium [25]. For undoped TiO_2, Figure 1b only shows a peak related to the Ti^{4+}. There is no obvious finding on spectra difference in detailed fine scanning on the Ti 2p region (Figure S1). The lithium doping on TiO_2 can result in the reduction from Ti^{4+} to Ti^{3+}, which can passivate the trap state or defects in TiO_2 films [22,23]. Correspondingly, this passivation can improve the charge transport in the lithium-treated TiO_2 [26].

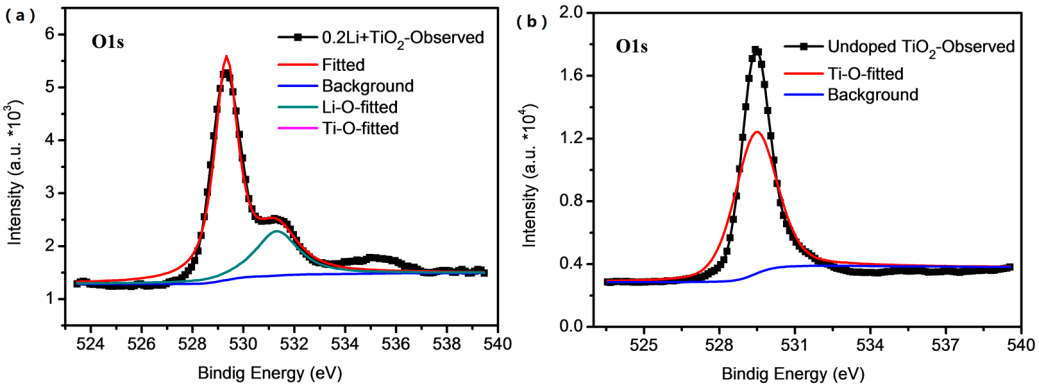

Figure 1. X-ray photoelectron spectroscopy. (**a**) The O1s peaks fitting for 0.2Li + TiO_2 sample. (**b**) The O1s peak fitting for undoped TiO_2 sample.

Figure 2a shows the XRD patterns of the as-deposited film and the annealed Sb_2S_3 film. It clearly shows that the as-deposited film is in amorphous state. For the sample annealed at 275 °C, the XRD pattern indicates a typical orthorhombic stibnite Sb_2S_3 phase (PDF#42-1393). The full width at half maxima (FWHM) for the peaks (310) is 0.360. Accordingly, the crystalline size calculated from the Debye-Scherrer formula for the peaks of (020), (110), (310) and (420) are 22.03, 24.46, 22.36 and 24.62 nm, respectively [27]. Figure 2b shows the SEM images of the surface morphology of the annealed Sb_2S_3 film. The uniform nano-crystalline of Sb_2S_3 films was formed after the thermal annealing. The thermal annealing process is accompanied by the obvious changes of crystalline and optical properties [4,8]. The Sb_2S_3 films annealed at 275 °C showed relatively small nanograins and homogenous surface morphology, which might reduce the leakage currents of devices. Figure S2 displays the EDX results. The atomic ratio of Sb:S is approaching 1:1.5, a bit larger than that of the ideal defect-free Sb_2S_3. The change of atomic ratio might come from the evaporation and the annealing process. It was reported that the thermal annealing of Sb_2S_3 films is accompanying with the sulfur diffusion, and with higher temperature and longer annealing time, the sulfur is more likely to diffuse into the environment with sulfur defects left in the films [8]. Moreover, because nanocrystalline Sb_2S_3 is enough for an efficient Sb_2S_3 solar cells [4], the annealing temperature of 275 °C was used for the crystallization in our experiment. From the EDX result the annealed Sb_2S_{3-x} film shows some sulfur-vacancies, suggesting the formation of N-type Sb_2S_3 absorber.

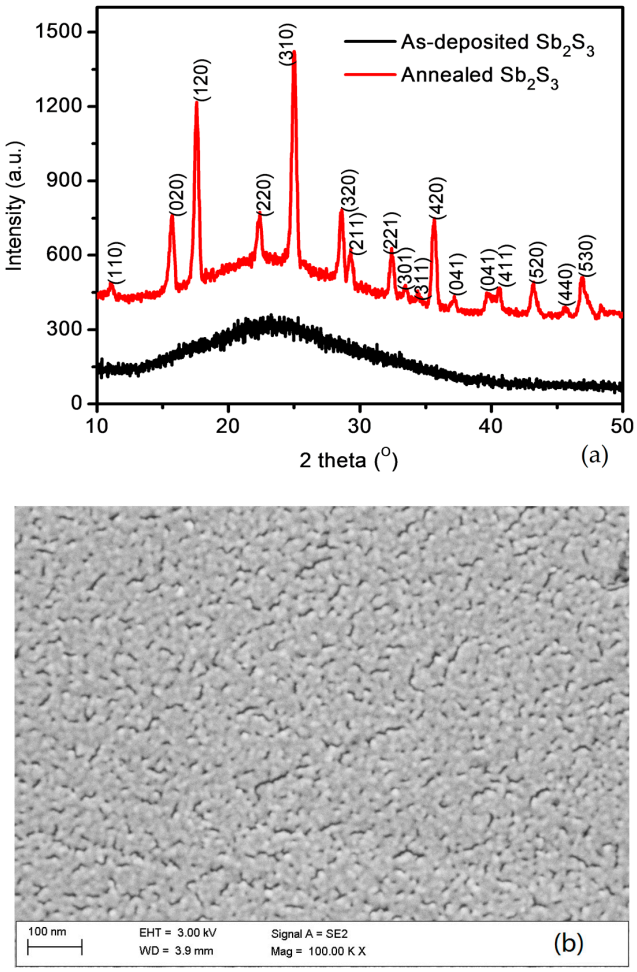

Figure 2. (**a**) XRD patterns for the Sb_2S_3 thin films and (**b**) the SEM of the surface morphology of the annealed Sb_2S_3 films.

Figure 3a shows the UV-visible light absorption of the annealed Sb_2S_3 film. The as-deposited amorphous state Sb_2S_3 film shows the color of yellow brown (Figure S3). After thermal annealing, the crystallized films become dark brown with the change of crystal structure (as shown in the inset picture). As shown in Figure 3a the absorption of the annealed Sb_2S_3 film covers the visible light region. The optical bandgap of the Sb_2S_3 thin film is estimated from transmittance spectrum in Figure 3b [28], where the threshold of the crystallized Sb_2S_3 films is 775 nm, indicating a bandgap E_g of 1.6 eV. However, even the threshold starts near 775 nm, the major absorption in the visible light region is mainly located in the range of 300 to 600 nm. Additionally, a small absorption tail is observed near infrared region. According to the XRD and SEM results, it must be the Urbach energy tail attributed to some amorphous state in the Sb_2S_3 films [4,29,30].

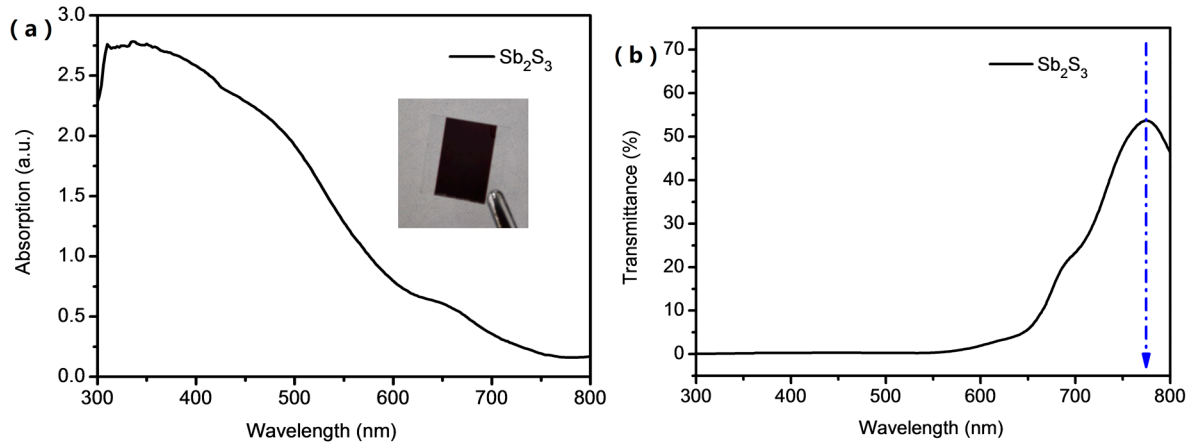

Figure 3. (**a**) UV-visible light absorption of the Sb_2S_3 thin films (the inset picture is the sample of the evaporated Sb_2S_3 thin film) and (**b**) transmittance spectrum of the Sb_2S_3 thin film.

To check the lithium doping TiO_2 effect on the photovoltaic performance of the Sb_2S_3 solar cells, the thermal evaporated Sb_2S_3 solar cells with the Li-doped TiO_2 electron transport layers were fabricated. Figure 4a shows the cross-section SEM image of the devices, and Figure 4b shows the configuration of the device in an architecture of FTO/compact TiO_2/mesoporous TiO_2/Sb_2S_3/HTM/Au. The thickness of mesoporous TiO_2/Sb_2S_3 is approximately 310 nm, where the mesoporous TiO_2 layer is 100 nm thick. In addition, the Spiro-OMeTAD layer is 200 nm thick. The cross-section SEM of the devices indicates the dense homogenous structures are formed in our experiment. In addition, then the photocurrent density–voltage characteristic was conducted under standard AM 1.5G one Sun illumination. Figure 5a shows the current density-voltage curves of the champion devices in each group. In the thermal-evaporated Sb_2S_3 solar cells with the undoped TiO_2, we reached a champion *PCE* of 3.74%, higher than that of the thermal-evaporated Sb_2S_3 solar cells previously reported (1.27% and 3.01%) [10,12]. It could be explained that the sulfur vacancies in the absorbing film resulted in higher concentration of electrons than that in defect-less or N-type Sb_2S_3 films, which benefits the overcoming of the heavy effective electron mass of the intrinsic Sb_2S_3 films. Additionally, from photovoltaic parameters in Table 1 and Figure S4 we clearly found that the photovoltaic performance of the devices was apparently improved with the increased doping of lithium on the mesoporous TiO_2 layers. The average V_{oc} of the Sb_2S_3 solar cells increased from 0.591 to 0.629 V with the increase lithium doping on meso-TiO_2, inferring less energy loss of the photo-excited electrons. At the same time, the average *PCE* increases from 1.79% to 4.04% with the increasing shunt resistances (R_{sh}) and the reduced series resistances (R_s). The *EQE* of Sb_2S_3 solar cells is shown in Figure 5b, and the calculated current density is accompanying with the tendency listed in Table 1. The lithium doping on the mesoporous TiO_2 can result in the enhanced electron extraction of TiO_2 [22,23]. Correspondingly, the faster electron extraction can happen from Sb_2S_3 to TiO_2 layer, which reduces the recombination of

electron-hole pairs in the absorbing layers. The statistics in Table S1 and Figure S3 further demonstrate that the devices based on the Li-doped TiO_2 are more repeatable, and their photovoltaic performance varies less than that based on the undoped TiO_2. The TiO_2 layers may become more conductive after Li-doping [22,23], thus the devices can achieve more effective charge extraction and the increase of the average short current density from 10.4 mA/cm^2 to 14.3 mA/cm^2, as well as the fill factors obviously improved from 0.28 to approximately 0.45. The Sb_2S_3 solar devices with undoped TiO_2 only showed an average *PCE* of 1.79%, while the devices with the highest lithium doping exhibited the best power conversion performance with a champion *PCE* of 4.42%, with the average *PCE* of 4.03%. The Sb_2S_3 solar cells based on 0.2Li + TiO_2 achieved a V_{oc} of 0.645 V (as shown in Figure S5), much higher than that with the undoped TiO_2.

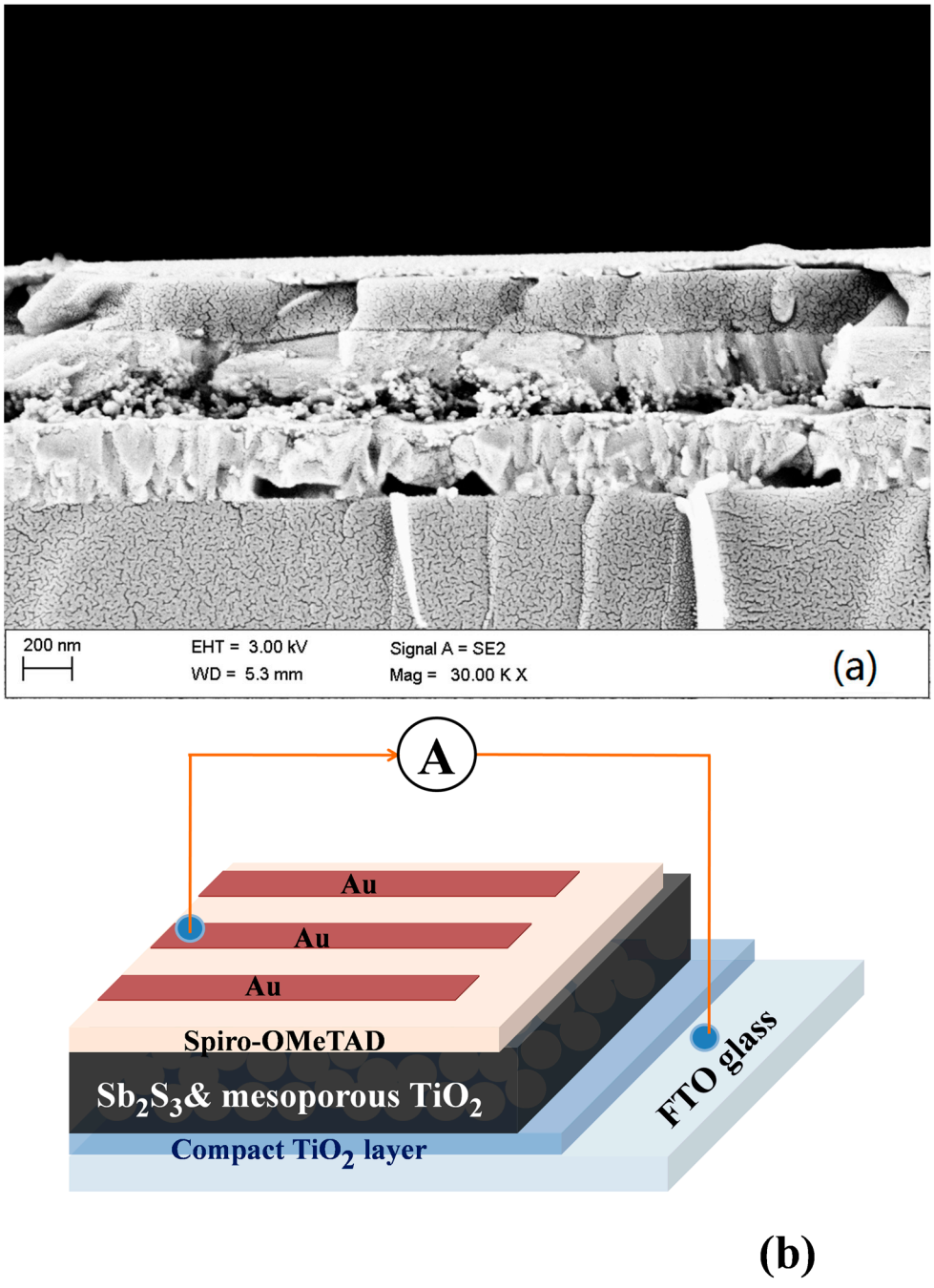

Figure 4. (**a**) Cross-section SEM of the Sb_2S_3 solar cells and (**b**) the configuration of the device.

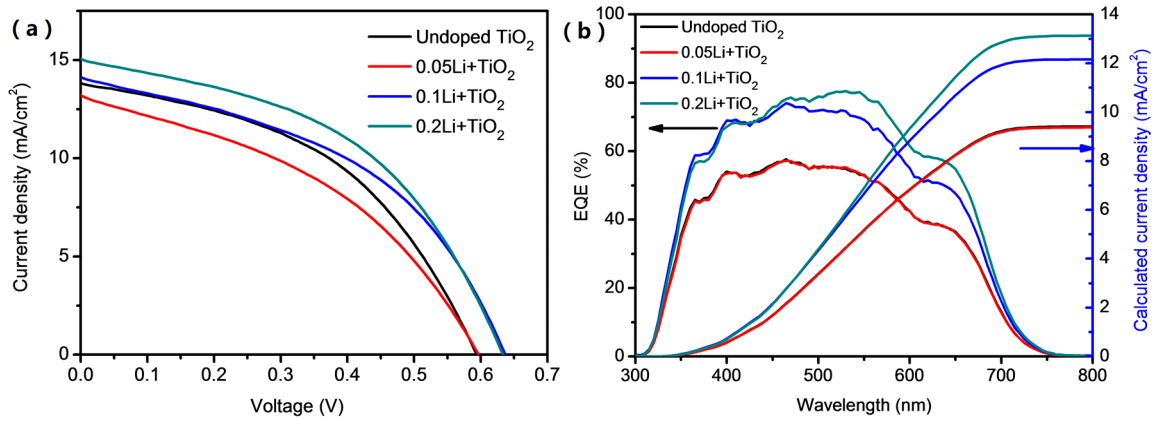

Figure 5. (**a**) The champion *J-V* curves of the devices based on different Li-doped TiO_2 and (**b**) EQE of the Sb_2S_3 solar cells.

Table 1. Photovoltaic parameters of the thermal-evaporated Sb_2S_3 solar cells based on different mesoporous TiO_2, measured under one Sun AM 1.5G illumination.

Mesoporous TiO_2		V_{oc} (V)	J_{sc} (mA/cm^2)	FF	*PCE* (%)	R_s (Ω cm^2)	R_{sh} (Ω·cm^2)
Undoped-TiO_2	champion	0.595	13.8	0.45	3.74	87	168
	Average	0.591	10.4	0.28	1.79	-	-
0.05Li-TiO_2	champion	0.595	13.2	0.41	3.19	57	100
	Average	0.606	10.9	0.30	1.93	-	-
0.1Li-TiO_2	champion	0.635	14.1	0.45	4.03	69	123
	Average	0.606	13.5	0.45	3.74	-	-
0.2Li-TiO_2	champion	0.635	15.0	0.46	4.42	68	149
	Average	0.629	14.3	0.45	4.03	-	-

Because Fermi level is one of the most important semiconductor properties of TiO_2, e.g., the difference of Fermi level in value between TiO_2 and the highest occupied molecular orbital level of the hole, transport layers can determine the open circuit voltage and charge extraction of solar cells [31]. We primarily characterized the Fermi level of the TiO_2 films to further evaluate the influence of Li-doping on the electron dynamics in the mesoporous TiO_2 layers. As shown in Figure 6a, the Mott–Schottky curves are fitted by the following equation:

$$\frac{1}{C^2} = \frac{2}{e\varepsilon\varepsilon_0 N_D}\left(E - E_f - \frac{kT}{e}\right) \quad (1)$$

where C represents the capacitance of the space charge region; E is applied potential, E_f is the Fermi level potential, and e, ε, ε_0, k, T represent the electron charge, the dielectric constants of materials, the vacuum permittivity, the Boltzmann constant and the absolute temperature, respectively. As shown in Figure 6a, when the potential is applied, the capacitance of the lithium-doped TiO_2 films changes faster than that of the undoped TiO_2, suggesting that a faster charge transport can happen from absorbing layer to electron transport layer in the solar cells. Besides the enhanced charge transport, the Fermi level must be another important reason for the improved photovoltaic performance. The fitted flat band potential for the Li-doped TiO_2 is -0.435 eV, for the undoped TiO_2 it is -0.361 eV. Correspondingly, an energy band diagram is presented in Figure 6b, where the difference of potentials between 0.2Li + TiO_2 and Spiro (ΔV_2) is higher than that between undoped TiO_2 and Spiro (ΔV_1). Therefore to some extent, the difference of energy bands can explain the improved V_{oc} of the Sb_2S_3 solar cells based on the Li-doped mesoporous TiO_2 layers.

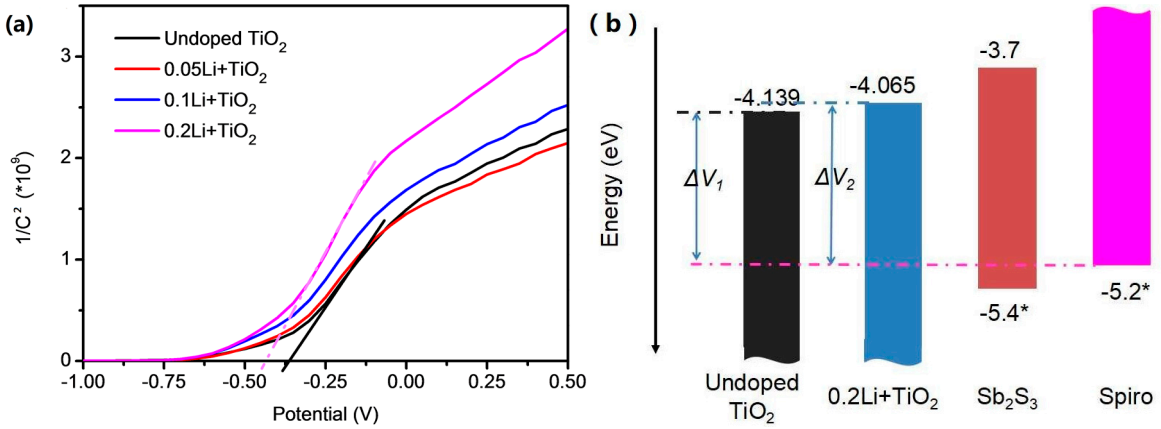

Figure 6. (**a**) Mott–Schottky curves of the mesoporous TiO_2 varying with Li-doping. (**b**) Energy band scheme [32].

4. Conclusions

In conclusion, we studied the effect of lithium-doping on charge transport properties of mesoporous TiO_2 layers for thermal-evaporated Sb_2S_3 thin film solar cells. XPS results demonstrated that lithium has been successfully introduced into the TiO_2. Based on the Mott-Schottky curves of the mesoporous TiO_2, it was found that lithium doping raised their platform potential and enhanced the charge transport. With the lithium doping on mesoporous TiO_2, the photovoltaic performance of the thermal-evaporated Sb_2S_3 solar cells has been dramatically improved. Compared with the solar cells using undoped TiO_2, the solar cells with Li-doped TiO_2 apparently demonstrated higher average *PCE*, from 1.79% to 4.04%, as well as the champion V_{oc} from 0.595 to 0.645 V, J_{sc} from 13.8 to 15.04 mA/cm^2 and the increased shut resistance. The Sb_2S_3 solar cells based on 0.2 M lithium-doped TiO_2 reached the champion *PCE* of 4.42%, which is the highest *PCE* among the reported thermal-evaporated Sb_2S_3 solar cells, and they showed less variation. This study provided a new strategy to improve the photovoltaic performance of Sb_2S_3-based solar cells.

Supplementary Materials: The following are available online at http://www.mdpi.com/1996-1944/11/3/355/s1.

Acknowledgments: This work was supported by Research and Development Program of China (Grant No. 2016YFB0402705), PhD Start-up Fund of Natural Science Foundation of Guangdong Province, China (A2017A030310375), National Natural Science Foundation of China (Grant No. 11575118) and Shenzhen Key Lab Fund (ZDSYS20170228105421966).

Author Contributions: Chunfeng Lan and Jingting Luo conceived and designed the experiments; Huabin Lan, Bo Fan, Huanxin Peng and Jun Zhao performed the experiments; Huibin Sun and Zhuanghao Zheng analyzed the data; Jingting Luo, Guangxing Liang and Ping Fan contributed reagents, materials and analysis tools; Chunfeng Lan, Jingting Luo, Ping Fan and Guangxing Liang wrote the paper.

Conflicts of Interest: The authors declare no conflict of interest.

References

1. Wang, L.; Li, D.B.; Li, K.H.; Chen, C.; Deng, H.X.; Gao, L.; Zhao, Y.; Jiang, F.; Li, L.Y.; Huang, F.; et al. Stable 6%-efficient Sb_2Se_3 solar cells with a ZnO buffer layer. *Nat. Energy* **2017**, *2*, 17046. [CrossRef]
2. Nasr, T.B.; Maghraoui-Meherzi, H.; Kamoun-Turki, N. First-principles study of electronic, thermoelectric and thermal properties of Sb_2S_3. *J. Alloys Compd.* **2016**, *663*, 123–127. [CrossRef]
3. Wang, X.M.; Li, J.M.; Liu, W.F.; Yang, S.F.; Zhu, C.F.; Chen, T.A. Fast Chemical Approach towards Sb_2S_3 Film with Large Grain Size for High-Performance Planar Heterojunction Solar Cells. *Nanoscale* **2017**, *9*, 3386–3390. [CrossRef] [PubMed]
4. Zheng, L.; Jiang, K.J.; Huang, J.H.; Zhang, Y.; Bao, B.; Zhou, X.Q.; Wang, H.J.; Guan, B.; Yang, L.M.; Song, Y.L. Solid-state nanocrystalline solar cells with an antimony sulfide absorber deposited by an in situ solid–gas reaction. *J. Mater. Chem. A* **2017**, *5*, 4791–4796. [CrossRef]

5. Shang, M.H.; Zhang, J.; Wei, S.H.; Zhu, Y.J.; Wang, L.; Hou, H.L.; Wu, Y.L.; Fujikawa, T.; Ueno, N. Bi-doped Sb_2S_3 for low effective mass and optimized optical properties. *J. Mater. Chem. C* **2016**, *4*, 5081–5090. [CrossRef]
6. Ito, S.; Tsujimoto, K.; Nguyen, D.C.; Manabe, K.; Nishino, H. Doping effects in Sb_2S_3 absorber for full-inorganic printed solar cells with 5.7% conversion efficiency. *Int. J. Hydrogen Energy* **2013**, *38*, 16749–16754. [CrossRef]
7. Choi, Y.C.; Lee, D.U.; Noh, J.H.; Kim, E.K.; Seok, S.I. Highly Improved Sb_2S_3 Sensitized-Inorganic–Organic Heterojunction Solar Cells and Quantification of Traps by Deep-Level Transient Spectroscopy. *Adv. Funct. Mater.* **2014**, *24*, 3587–3592. [CrossRef]
8. Marquina, R.G.S.; Sanchez, T.G.; Mathews, N.R.; Mathew, X. Vacuum coated Sb_2S_3 thin films: Thermal treatment and the evolution of its physical properties. *Mater. Res. Bull.* **2017**, *90*, 285–294. [CrossRef]
9. Garcia, R.G.A.; Avendaño, C.A.M.; Mou, P.; Delgado, F.P.; Mathews, N.R. Antimony sulfide (Sb_2S_3) thin films by pulse electrodeposition: Effect of thermal treatment on structural, optical and electrical properties. *Mater. Sci. Semicond. Process.* **2016**, *44*, 91–100. [CrossRef]
10. Chen, X.; Li, Z.Q.; Zhu, H.B.; Wang, Y.; Liang, B.L.; Chen, J.W.; Xu, Y.; Mai, Y.H. CdS/Sb_2S_3 heterojunction thin film solar cells with a thermally evaporated absorber. *J. Mater. Chem. C* **2017**, *5*, 9421. [CrossRef]
11. Cardoso, J.C.; Grimes, C.A.; Feng, X.J.; Zhang, X.Y.; Komarneni, S.; Zanoni, M.V.B.; Bao, N.Z. Fabrication of coaxial TiO_2/Sb_2S_3 nanowire hybrids for efficient nanostructured organic–inorganic thin film photovoltaics. *Chem. Commun.* **2012**, *48*, 2818–2820. [CrossRef] [PubMed]
12. Escorcia-García, J.; Becerra, D.; Nair, M.T.S.; Nair, P.K. Heterojunction CdS/Sb_2S_3 solar cells using antimony sulfide thin films prepared by thermal evaporation. *Thin Solid Films* **2014**, *569*, 28–34. [CrossRef]
13. Mayon, Y.O.; White, T.P.; Wang, R.; Yang, Z.; Catchpole, K.R. Evaporated and solution deposited planar Sb_2S_3 solar cells: A comparison and its significance. *Phys. Status Solidi A* **2016**, *213*, 108–113. [CrossRef]
14. Zimmermann, E.; Pfadler, T.; Kalb, J.; Dorman, J.A.; Sommer, D.; Hahn, G.; Weickert, J.; Schmidt-Mende, L. Toward High Efficiency Solution-Processed Planar Heterojunction Sb_2S_3 Solar Cells. *Adv. Sci.* **2015**, *2*, 1500059. [CrossRef] [PubMed]
15. Pérez-Martínez, D.; Gonzaga-Sánchez, J.D.; Bray-Sánchez, F.D.; Vázquez-García, G.; Escorcia-García, J.; Nair, M.T.S.; Nair, P.K. Simple solar cells of 3.5% efficiency with antimony sulfide-selenide thin films. *Phys. Status Solidi RRL* **2016**, *10*, 388–396. [CrossRef]
16. O'Mahony, F.T.F.; Lutz, T.; Guijarro, N.; Gómez, R.; Haque, S.A. Electron and hole transfer at metal oxide/Sb_2S_3/spiro-OMeTAD heterojunctions. *Energy Environ. Sci.* **2012**, *5*, 9760–9764. [CrossRef]
17. Boix, P.P.; Larramona, G.; Jacob, A.; Delatouche, B.; Mora-Seró, I.; Bisquert, J. Hole Transport and Recombination in All-Solid Sb_2S_3-Sensitized TiO_2 Solar Cells Using CuSCN As Hole Transporter. *J. Phys. Chem. C* **2012**, *116*, 1579–1587. [CrossRef]
18. Itzhaik, Y.; Niitsoo, O.; Page, M.; Hodes, G. Sb_2S_3-Sensitized Nanoporous TiO_2 Solar Cells. *J. Phys. Chem. C* **2009**, *113*, 4254–4256. [CrossRef]
19. Parize, R.; Katerski, A.; Gromyko, I.; Rapenne, L.; Roussel, H.; Kärber, E.; Appert, E.; Krunks, M.; Consonni, V. Phosphonic Acid and Lithium Salt as Effective p-Dopants to Oxidize Spiro-OMeTAD for Mesoscopic Sb_2S_3 Solar Cells. *J. Phys. Chem. C* **2017**, *121*, 9672–9680. [CrossRef]
20. Yuan, S.J.; Deng, H.; Dong, D.D.; Yang, X.K.; Qiao, K.K.; Hu, C.; Song, H.B.; Song, H.S.; He, Z.B.; Tang, J. Efficient planar antimony sulfide thin film photovoltaics with large grain and preferential growth. *Sol. Energy Mater. Sol. Cells* **2016**, *157*, 887–893. [CrossRef]
21. Zhang, H.Y.; Shi, J.J.; Xu, X.; Zhu, L.F.; Luo, Y.H.; Li, D.M.; Meng, Q.B. Mg-doped TiO_2 boosts the efficiency of planar perovskite solar cells to exceed 19%. *J. Mater. Chem. A* **2016**, *4*, 15383. [CrossRef]
22. Giordano, F.; Abate, A.; Baena, J.P.C.; Saliba, M.; Matsui, T.; Im, S.H.; Zakeeruddin, S.M.; Nazeeruddin, M.K.; Hagfeldt, A.; Graetzel, M. Enhanced electronic properties in mesoporous TiO_2 via lithium doping for high-efficiency perovskite solar cells. *Nat. Commun.* **2016**, *7*, 10379. [CrossRef] [PubMed]
23. Liu, D.T.; Li, S.B.; Zhang, P.; Wang, Y.F.; Zhang, R.; Sarvari, H.; Wang, F.; Wu, J.; Wang, Z.M.; Chen, Z.D. Efficient planar heterojunction perovskite solar cells with Li-doped compact TiO_2 layer. *Nano Energy* **2017**, *31*, 462–468. [CrossRef]
24. Zhou, H.W.; Shi, Y.T.; Dong, Q.S.; Zhang, H.; Xing, Y.J.; Wang, K.; Du, Y.; Ma, T.L. Hole-conductor-free, metal-electrode-free TiO_2/$CH_3NH_3PbI_3$ heterojunction solar cells based on a low-temperature carbon electrode. *J. Phys. Chem. Lett.* **2014**, *5*, 3241–3246. [CrossRef] [PubMed]

25. Södergren, S.; Siegbahn, H.; Rensmo, H.; Lindström, H.; Hagfeldt, A.A.; Lindquist, S.E. Lithium Intercalation in Nanoporous Anatase TiO_2 Studied with XPS. *J. Phys. Chem. B* **1997**, *101*, 3087–3090. [CrossRef]
26. Bouattour, S.; Kallel, W.; Rego, A.M.B.D.; Ferreira, L.F.V.; Machado, I.F.; Boufi, S. Li-doped nanosized TiO_2 powder with enhanced photocalatylicacivity under sunlight irradiation. *Appl. Organomet. Chem.* **2010**, *24*, 692–699. [CrossRef]
27. Cullity, B.D.; Stock, S.R. *Elements of X-Ray Diffraction*, 3rd ed.; Prentice-Hall: Upper Saddle River, NJ, USA, 2001; pp. 167–171.
28. Liang, G.-X.; Fan, P.; Luo, J.-T.; Gu, D.; Zheng, Z.-H. A promising unisource thermal evaporation for in situ fabrication of organolead halide perovskite $CH_3NH_3PbI_3$ thin film. *Prog. Photovolt. Res. Appl.* **2015**, *23*, 1901–1907. [CrossRef]
29. Hassanien, A.S.; Akl, A.A. Influence of composition on optical and dispersion parameters of thermally evaporated non-crystalline Cd50S50−xSex thin films. *J. Alloys Compd.* **2015**, *648*, 280–290. [CrossRef]
30. Perales, F.; Lifante, G.; Agullórueda, F.; De, H.C. Optical and structural properties in the amorphous to polycrystalline transition in Sb_2S_3 thin films. *J. Phys. D: Appl. Phys.* **2007**, *40*, 2440–2444. [CrossRef]
31. Wang, K.; Shi, Y.T.; Li, B.; Zhao, L.; Wang, W.; Wang, X.Y.; Bai, X.G.; Wang, S.F.; Hao, C.; Ma, T.L. Amorphous Inorganic Electron-Selective Layers for Efficient Perovskite Solar Cells: Feasible Strategy Towards Room Temperature Fabrication. *Adv. Mater.* **2016**, *28*, 1891–1897. [CrossRef] [PubMed]
32. Zhang, Y.; Li, J.; Jiang, G.; Liu, W.; Yang, S.; Zhu, C.; Chen, T. Selenium-Graded $Sb_2(S_{1-x}Se_x)_3$ for Planar Heterojunction Solar Cell Delivering a Certified Power Conversion Efficiency of 5.71%. *Sol. RRL* **2017**, *1*, 1700017. [CrossRef]